Role of the Drake Passage in Controlling the Stability of the Ocean's Thermohaline Circulation

WILLEM P. SIJP AND MATTHEW H. ENGLAND

Centre for Environmental Modelling and Prediction, School of Mathematics, University of New South Wales, Sydney, New South Wales, Australia

(Manuscript received 8 June 2004, in final form 24 October 2004)

ABSTRACT

The role of a Southern Ocean gateway in permitting multiple equilibria of the global ocean thermohaline circulation is examined. In particular, necessary conditions for the existence of multiple equilibria are studied with a coupled climate model, wherein stable solutions are obtained for a range of bathymetries with varying Drake Passage (DP) depths. No transitions to a Northern Hemisphere (NH) overturning state are found when the Drake Passage sill is shallower than a critical depth (1100 m in the model described herein). This preference for Southern Hemisphere sinking is a result of the particularly cold conditions of the Antarctic Bottom Water (AABW) formation regions compared to the NH deep-water formation zones. In a shallow or closed DP configuration, this forces an exclusive production of deep/bottom water in the Southern Hemisphere. Increasing the depth of the Drake Passage sill causes a gradual vertical decoupling in Atlantic circulation, removing the influence of AABW from the upper 2000 m of the Atlantic Ocean. When the DP is sufficiently deep, this shifts the interaction between a North Atlantic Deep Water (NADW) cell and an AABW cell to an interaction between an (shallower) Antarctic Intermediate Water cell and an NADW cell. This latter situation allows transitions to a Northern Hemisphere overturning state.

1. Introduction

The gradual deepening of a southern gateway since the Oligocene is thought to have had an influence on Antarctic climate (Kennett 1977). Toggweiler and Bjornsson (2000) and Sijp and England (2004, hereafter SE2004) use climate models to suggest that Southern Hemisphere (SH) climate change due to the opening of a Drake Passage (DP) is relatively abrupt, in that it occurs once even a shallow DP is established. They based this conclusion on findings that the SH climate for a shallow DP experiment is very similar to that of today, yet markedly different to the closed DP climate. The DP closed (DP_{clsd}) experiment in SE2004 exhibits large SH overturning and no North Atlantic Deep Water (NADW) formation. Southern Hemisphere sinking is particularly vigorous in the DP_{clsd} experiment, where 55 Sv (1 Sv $\equiv 10^6$ m^3 s^{-1}) sink off Antarctica. However, no attempts were made in either SE2004 or Toggweiler and Bjornsson (2000) to excite transitions to a possible Northern Hemisphere (NH) overturning state. Here we examine the existence of multiple equilibria for a range of DP depths, including one that is closed, in a coupled climate model.

Bryan (1986) showed that stable interhemispheric overturning states with predominant sinking in one hemisphere could be obtained in a rectangular basin geometry under symmetric surface forcing. The density contrast between the antipodean deep-water formation regions determines the strength and polarity of this circulation. For example, an SH sinking state corresponds to higher SH surface densities. However, a striking simplification of Bryan's geometry is the absence of a circumpolar ocean at the latitudes of the DP. In the real ocean, this unbounded region constitutes an obstruction to meridional geostrophic flow to higher southern latitudes (Toggweiler and Samuels 1995). As a result of the DP gap, ocean ventilation of Antarctic Intermediate Water (AAIW) occurs to depths of around 1000 m (e.g., Cox 1989). Saenko et al. (2003) demonstrate the importance of the relationship between densities in the AAIW formation regions (ρ_{AAIW}) and those in the NADW formation regions (ρ_{NADW}) in determining the

Corresponding author address: Willem P. Sijp, School of Mathematics, University of New South Wales, Sydney, NSW 2052, Australia.
E-mail: wsijp@maths.unsw.edu.au

global ocean meridional overturning (MOT). For example, an SH sinking state can be obtained when freshwater (FW) is extracted from the AAIW formation regions such that $\rho_{AAIW} > \rho_{NADW}$. Unlike Bryan (1986) and the closed DP case of SE2004, this SH state consists of an AAIW reverse cell overlying a circulation of Antarctic Bottom Water (AABW) in the Atlantic below 2000-m depth. The AAIW reverse cell favors an enhanced FW flux into the Atlantic, transporting relatively saline low-latitude waters out of the Atlantic near the surface while importing fresher AAIW. Saenko et al. (2003) show that the resulting freshening of the North Atlantic (NA) prevents ρ_{NADW} from rising above ρ_{AAIW} after cessation of the FW extraction, thus yielding a stable NADW "off" state.

While it is clear that the ocean is characterized by an interhemispheric competition for ventilation dominance, the role of SH–NH landmass asymmetry in setting stable climate equilibria remains relatively unexplored. In this study we examine the role of the depth of the DP sill in permitting multiple equilibria in the ocean's thermohaline circulation (THC). It will be shown that the depth of the DP sill plays a fundamental role in determining the relative importance of the three global water masses (AABW, AAIW, and NADW) in setting the global ocean THC. AABW mostly forms in the Ross and Weddell Seas, spreading below NADW, whereas intensive AAIW formation is thought to occur in a localized region around the tip of South America (McCartney 1977; England et al. 1993). A schematic of these formation regions is indicated in Fig. 1. We will show that the dominant SH water mass formation site shifts gradually from AABW to AAIW with deepening DP, thus shifting the thermohaline circulation control from ρ_{NADW} versus ρ_{AABW} (DP_{clsd}) to ρ_{NADW} versus ρ_{AAIW} (DP_{open}). Different surface density conditions in these respective areas make the latter density contrast more favorable to a NADW "on" state, as seen in today's climate.

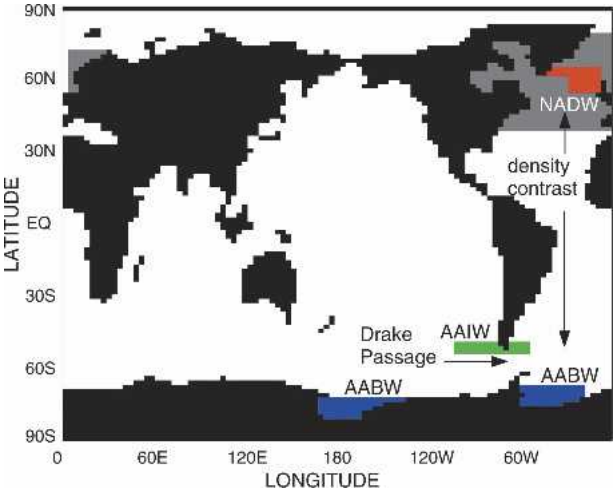

FIG. 1. Model domain and primary water mass formation regions. The gray and red areas in the North Atlantic combined indicate the region used in FW extraction under forcings 1 and 2. The density contrast between NH and SH sinking regions determines the structure of the Atlantic MOT. With a deepening DP, the importance of the AABW formation regions shifts to the AAIW regions. Formation regions for AABW (blue), AAIW (green), and NADW (red) are also indicated.

2. Methodology

a. The coupled model

The coupled model used in this study is described in detail in Weaver et al. (2001). The model comprises an ocean general circulation model coupled to a simplified atmospheric model and a dynamic–thermodynamic sea ice model. The components of the model have a global domain with a horizontal resolution of 1.8° latitude × 3.6° longitude. The ocean model uses constant horizontal mixing with no eddy-induced transport included in the main set of experiments. Vertical mixing is achieved using a diffusivity that increases with depth, taking a value of 0.6 $cm^2\ s^{-1}$ at the surface and 1.6 $cm^2\ s^{-1}$ at the bottom. The wind forcing is taken from the National Centers for Environmental Prediction–National Center for Atmospheric Research (NCEP–NCAR) reanalysis fields (Kalnay et al. 1996), which are averaged over the period of 1958–97 to form a seasonal cycle from the monthly fields. There is a parameterization of brine rejection during sea ice formation (after Duffy and Caldeira 1997). The atmospheric model calculates surface heat and freshwater fluxes, advects and diffuses moisture, and only diffuses heat. For a full model description the reader is referred to Weaver et al. (2001).

b. Experimental design

Our experiments are based on a series of 2100-yr integrations from idealized initial conditions in six bathymetries that are set up identically, with the exception of the DP sill depth. Table 1 lists the DP sill depths considered in this study, ranging from 0 (DP_{clsd}) down to 2316 (DP_{open}). We then apply FW perturbations to these experiments in order to obtain states with no NADW formation, and, if possible, states with NADW formation. All of the experiments can be perturbed to yield a state with no NADW formation. This state is denoted by $NADW_{off}$. Some experiments exhibit a steady state with NADW overturn, these are denoted by $NADW_{on}$. We denote the FW perturbations by forc-

TABLE 1. List of all experiments and DP depth. The third column indicates whether a $NADW_{on}$ state is found. The last three columns show Atlantic AABW inflow, AABW upwelling across 2000-m depth, and the strength of the AAIW reverse cell in the Atlantic for the $NADW_{off}$ states (for definitions of the MOT quantities see section 2c). All transport values are given in Sv (1 Sv $\equiv 10^6$ m^3 s^{-1}).

Experiment	DP depth (m)	NADW exists?	AABW inflow	AABW upwelling	AAIW reverse cell
DP_{clsd}	0	No	12.5	12.5	—
DP_{690}	690	No	5.3	5.0	5.6
DP_{896}	896	No	5.0	3.4	7.1
DP_{1128}	1128	Yes	5.0	2.3	8.6
DP_{1386}	1386	Yes	4.9	1.5	9.7
DP_{open}	2316	Yes	4.6	0.8	10.4

ing 1 and forcing 2 (shown in Fig. 4b). These perturbations involve the addition of an extra term to the usual surface salinity flux field, which is otherwise determined by internal model factors such as precipitation, evaporation, sea ice growth/melt, river runoff, and runoff outside of river mouths. This artificial FW loss is applied uniformly inside the gray and red regions shown in Fig. 1. The two forcings vary to simulate pulses of FW extraction from the North Atlantic to excite possible transitions to stable NADW formation states. Forcing 1 consists of a linear decrease from 0 to -2.25 mm day^{-1} at year 150, returning to zero perturbation by year 300. This is equivalent to an integrated North Atlantic FW loss of 0.7 Sv at the peak of the freshwater anomaly. Forcing 2 is double the intensity of forcing 1.

We use identical seasonal wind stress fields throughout the experiments. We thus do not examine the effect of a varying wind stress in driving the NH overturning. The so-called "Drake Passage effect," where winds over the Southern Ocean control, in part, the rate of NADW production, has been examined in many studies (e.g., Toggweiler and Samuels 1995; Rahmstorf and England 1997; Tsujino and Suginohara 1999; Klinger et al. 2004). There is still some debate as to whether this control is via mechanical (Toggweiler and Samuels 1995) or wind-driven buoyancy effects (Gnanadesikan and Hallberg 2000). It is noted that the DP effect requires a DP sill depth of ~1500–2000 m, which is much deeper than our shallow DP experiments. In addition, with fixed seasonal wind stress forcing in our experiments, the DP effect is beyond the scope of this study. We will explain model MOT behavior in terms of buoyancy effects, which is a natural consequence of the buoyancy perturbations employed in our experimental design.

c. *Overturning diagnostics*

To study the dynamic behavior of the Atlantic MOT in response to the FW perturbations, we record the NADW formation rate as the maximum value of the MOT in the downwelling branch of the North Atlantic (see Fig. 5). We also record the following MOT quantities.

1) Atlantic AAIW reverse cell strength: In the $NADW_{off}$ states of all of the experiments except DP_{clsd}, the AAIW reverse cell and the AABW cell are separated by a local minimum of the absolute strength of the MOT, occurring at around 2000-m depth (see Figs. 3b–f). We measure the strength of the AAIW reverse cell by taking the difference between this absolute minimum and the peak magnitude of the AAIW cell at 30°S (usually occurring in the upper 1000 m if a reverse cell exists; Figs. 3b–f indicate this cell strength).
2) NADW outflow: This is taken to be the maximum of the MOT in the Atlantic sector at 33°S (see Fig. 5), normally occurring at around 1600-m depth.
3) Atlantic AABW inflow: This is taken as the maximum magnitude of the abyssal MOT cell at 33°S in the Atlantic sector. This measures the amount of inflow of AABW into the Atlantic (see Fig. 3).
4) Atlantic AABW upwelling: This is taken to be the magnitude of upwelling transport across a 1980-m depth in the Atlantic sector between 33°S and 59°N (see Fig. 3). This measures the net amount of water that is upwelled across 2000-m depth in the Atlantic.

3. Results

a. *$NADW_{off}$ states*

We begin by analyzing the equilibrium overturning of the respective $NADW_{off}$ states. Figure 2 shows the global MOT for DP_{clsd}, DP_{690}, and the $NADW_{off}$ state of DP_{open} taken from 10-yr means at the end of the unperturbed model integrations. It can be seen that DP_{clsd} exhibits a large interhemispheric overturning cell (55 Sv) originating in the SH. When the DP is opened to 690-m depth, with still no NADW formation, a dramatic change in MOT occurs in the SH—the Deacon Cell appears,[1] which is characterized by surface Ekman transport that is balanced by a deeper return flow beneath the DP sill, and the AABW production rate drops from 55 to only

[1] It is noted that the Deacon Cell mostly disappears in density coordinates (Döös and Webb 1994) and, so, does not play a major role in water mass modification in the Southern Ocean.

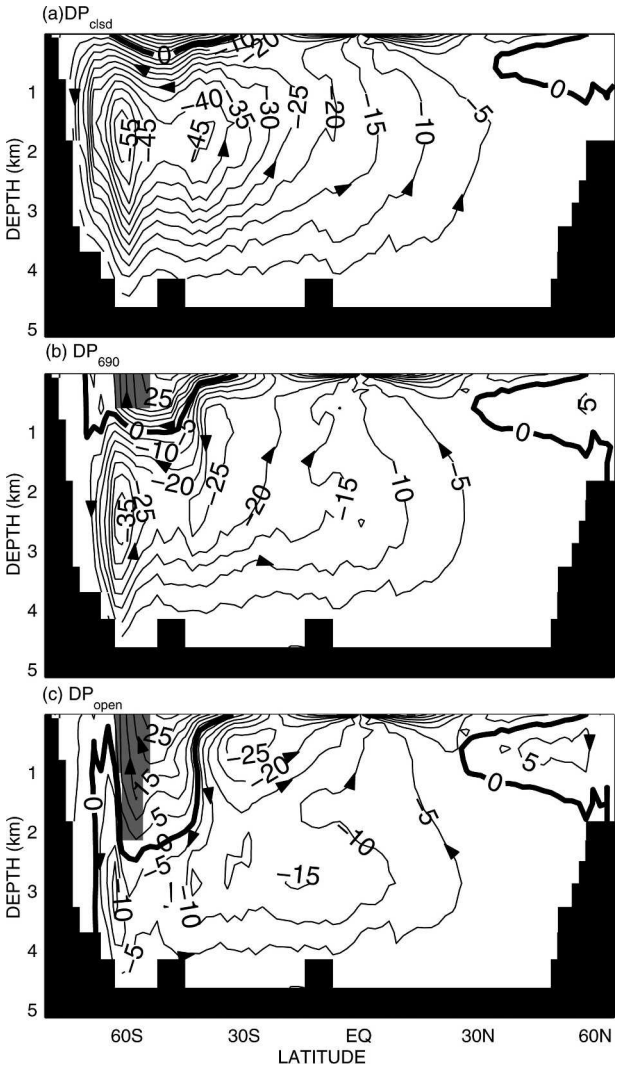

FIG. 2. Global meridional overturning streamfunction (10-yr average) for the $NADW_{off}$ states in (a) DP_{clsd}, (b) DP_{690}, and (c) DP_{open} bathymetries. Values are given in Sv. The outline of the DP gap is indicated by shading.

35 Sv. This reduction in AABW is independent of any interhemispheric density forcing, and is entirely due to the emergence of a DP gap. The DP_{open} case shows that further deepening of DP results in a deeper Deacon Cell and a further reduction of the AABW cell down to its preindustrial value of ~15 Sv (Broecker et al. 1999).

To examine the relative roles of temperature and salinity in determining the vigorous sinking of AABW in the closed DP case, we have run experiments where salinity is held constant at 34.72 psu. This yields similar results to the standard DP_{clsd} case, with an AABW overturning of around 60 Sv, indicating that the large SH overturning cell is thermally driven.

Figure 3 shows the Atlantic MOT for the $NADW_{off}$ states for each of the DP bathymetry experiments taken from 10-yr means. Figure 3a shows that in DP_{clsd} the SH AABW cell extends to the high northern latitudes and dominates all depth levels of the Atlantic. A second water mass (AAIW) appears when a shallow (690 m) DP gap is introduced (Fig. 3b). Waters in the upper 2000 m of the Atlantic now originate from AABW upwelling across 2000 m (5.6 Sv) and AAIW flowing across 30°S (5 Sv). The AAIW component forms a reverse cell, enveloped by a larger AABW cell. Figures 3b–f show that with a deepening DP the dominant ventilation in the upper 2000 m of the Atlantic shifts gradually from AABW upwelling to AAIW inflow. Note also the gradual vertical partitioning across 2000 m in the Atlantic MOT as DP deepens—two vertically stacked SH cells emerge (DP_{open}) from one SH AABW cell (DP_{clsd}). Another interesting feature of Fig. 3 is that once a shallow DP gap is established, AABW inflow remains relatively constant (around 5 Sv, see Table 1), even as DP is deepened.

It may be noted that North Atlantic freshwater fluxes (figure not shown) are reasonably similar for both the $NADW_{off}$ and the $NADW_{on}$ states in DP_{open}. Yet we will see later that sea surface salinity is substantially different between $NADW_{on}$ and $NADW_{off}$ states, regardless of DP bathymetry. This indicates that surface circulation, not FW fluxes, determines sea surface salinity (SSS) to a large extent in the North Atlantic. The North Atlantic horizontal circulation field is very similar for the $NADW_{off}$ case in DP_{open} and the steady-state (i.e., $NADW_{off}$) field in DP_{clsd} (figure not shown). In fact, all $NADW_{off}$ cases show a highly similar pattern of horizontal circulation in the North Atlantic, regardless of DP geometry.

b. Response to FW perturbations

Figure 4 shows the transient response of NADW production to the FW perturbations for the six bathymetries. For each bathymetry the $NADW_{off}$ state is used as the initial condition. The time series shown in Fig. 4a correspond to the NADW production for DP_{open}, DP_{1386}, and DP_{1128} under forcing 1 and DP_{clsd}, DP_{690}, and DP_{896} under forcing 2. The time series show a successful transition to a $NADW_{on}$ state for DP_{open}, DP_{1386}, and DP_{1128} under the moderate FW perturbation of forcing 1. In contrast, we fail to obtain stable $NADW_{on}$ states for the remaining bathymetries DP_{clsd}, DP_{690}, and DP_{896} under the stronger FW extraction of forcing 2. We have also subjected these experiments to an even stronger and more prolonged forcing (figure not shown) that is applied concurrently with an opposite sign in each hemisphere. Although AABW is fully suppressed for a prolonged period of time in these ex-

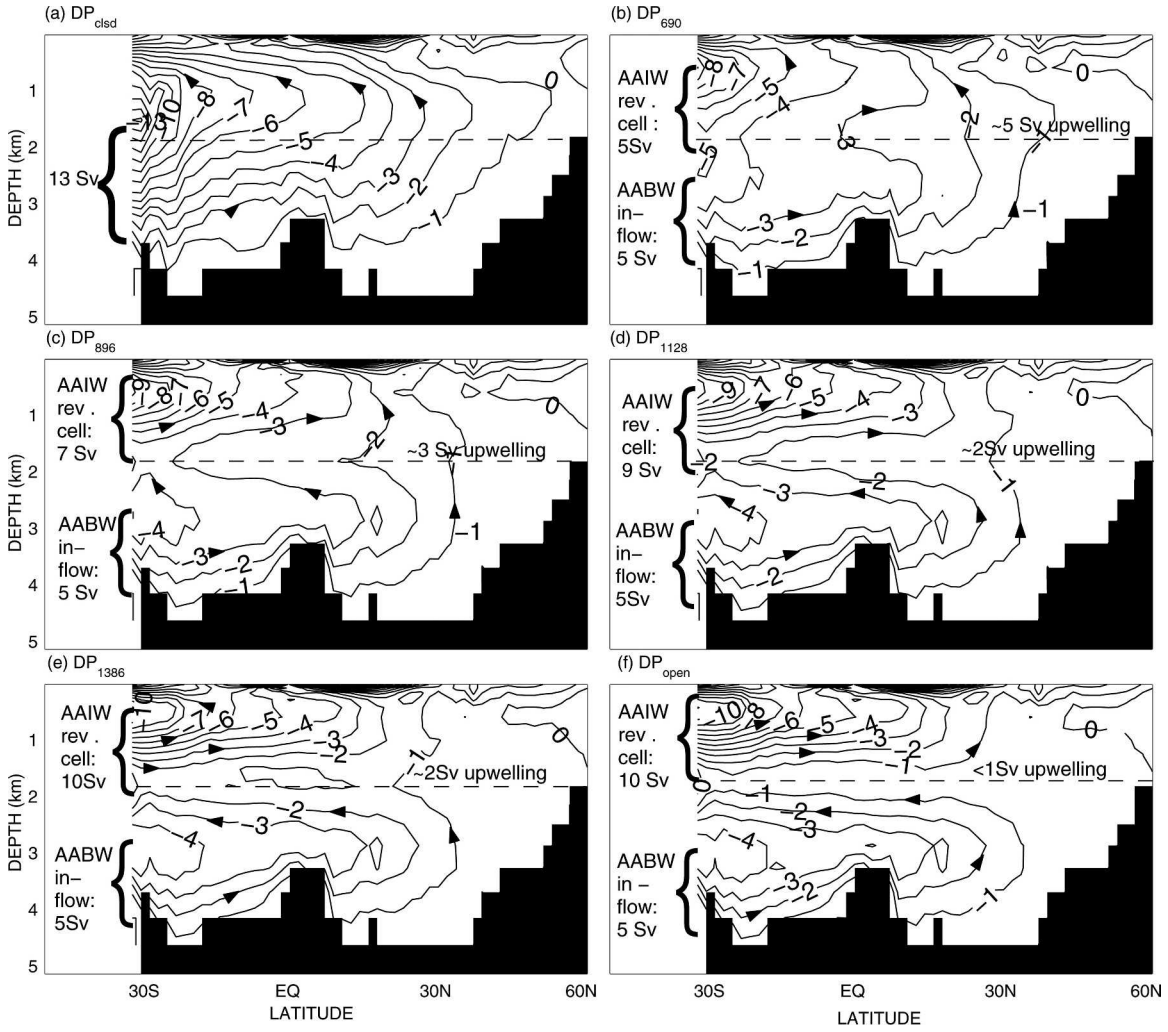

FIG. 3. Atlantic meridional overturning streamfunction (10-yr average) for the $NADW_{off}$ states in (a) DP_{clsd}, (b) DP_{690}, (c) DP_{896}, (d) DP_{1128}, (e) DP_{1386}, and (f) DP_{open} bathymetries. Values are given in Sv.

periments, the MOT returns to an SH polarity after removal of the FW forcing, with no sustenance of NADW. Finally, we note the relatively slow decay of NADW in DP_{896}. There appears to be a threshold depth of the DP sill above which NADW cannot be sustained. The DP_{896} case would appear to lie close to this threshold in our model.

It is worth briefly discussing the NA MOT obtained for the $NADW_{on}$ states. Figure 5 shows the Atlantic MOT for (a) DP_{1128} and (b) DP_{open} in the $NADW_{on}$ states. Although DP_{1128} exhibits less NADW formation and outflow compared to DP_{open}, there is a general similarity in overturning patterns between the two experiments. NADW formation and outflow are reduced in DP_{1128} by ~2 and ~4 Sv, respectively, compared to DP_{open}. This reduction in NADW outflow will be shown to be consistent with a reduction in the northward branching of AAIW as DP progressively deepens (see section 4). By conservation of mass, reduced AAIW northward flow must result in reduced NADW outflow.

Figure 6 shows several other MOT quantities in DP_{clsd} and DP_{1128} that are measured during the model response to forcing 2, designed to excite a transition from a $NADW_{off}$ state to a $NADW_{on}$ state. Unlike DP_{690}, DP_{1128} exhibits a transition to a stable $NADW_{on}$ state. During sustenance of NADW, DP_{1128} shows a collapsed AAIW reverse cell (Fig. 6c), no AABW upwelling across 2000-m depth in the Atlantic sector (Fig. 6d), and a steady AABW inflow of ~4 Sv (Fig. 6e). In contrast, NADW cannot be sustained in DP_{690}. Immediately after the end of the FW extraction period AABW inflow starts to recover to its previous value of >5 Sv. Several hundred years later, AABW upwelling

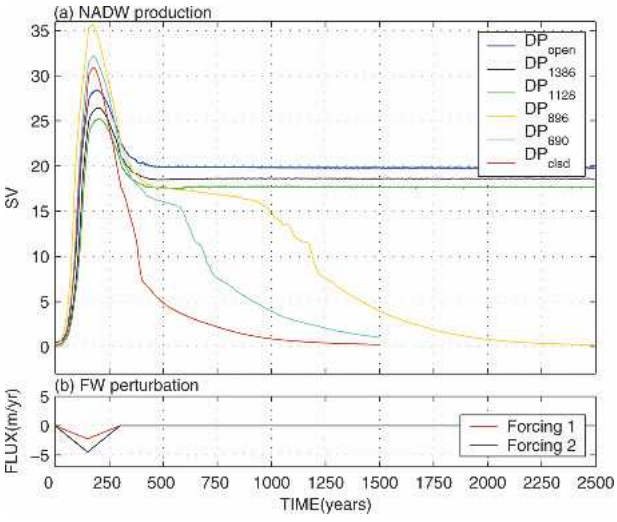

FIG. 4. (a) NADW production rate vs time in the series of experiments conducted to excite transitions to $NADW_{on}$ states. (b) Time history of FW perturbations in forcings 1 and 2. The time series of NADW production in (a) exhibit a successful transition to $NADW_{on}$ states for DP_{1128} (green), DP_{1386} (black), and DP_{open} (blue) in response to forcing 1. Even under the stronger forcing 2 there is no excitation of a transition to an $NADW_{on}$ state for DP_{clsd} (red), DP_{690} (cyan), and DP_{896} (yellow). Note that here DP_{open}, DP_{1386}, and DP_{1128} are forced with forcing 1 [red in (b)], whereas DP_{clsd}, DP_{690}, and DP_{896} are forced with the stronger perturbation of forcing 2 [black in (b)].

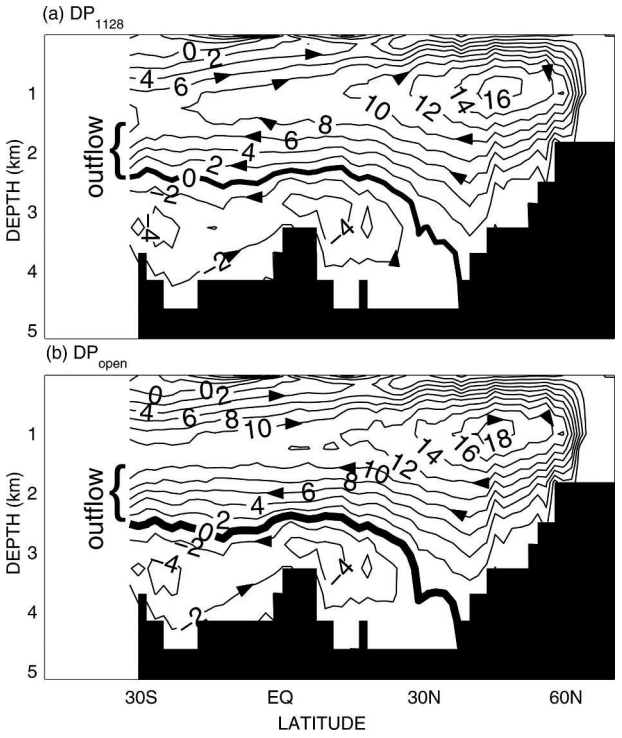

FIG. 5. Atlantic meridional overturning streamfunction (10-yr average) for the $NADW_{on}$ states in bathymetries (a) DP_{1128} and (b) DP_{open}. Values are given in Sv. In this study the NADW formation rate is defined as the maximum of the downwelling branch of the MOT cell in the NA. NADW outflow is, as indicated, the maximum MOT at 33°S.

across 2000 m is reestablished, as is the AAIW reverse cell. By this time, NADW is nearing its final collapse and return to a steady $NADW_{off}$ state.

Figure 7 shows the temperature and salinity properties at the sea surface in the NADW, AABW, and AAIW sinking regions for the nine different equilibria. $NADW_{on}$ states are shown for DP_{open}, DP_{1386}, and DP_{1128}, and the $NADW_{off}$ states are shown for all bathymetries from DP_{open} to DP_{clsd}. The colors correspond to the water mass formation regions shown in Fig. 1. The variation of ρ_{AABW} (blue) is relatively small among the equilibria, as it is for ρ_{AAIW} (green). Howewever, for ρ_{NADW} (red) there are two distinct clusters of points. One cluster is characterized by temperature (T) and salinity (S) of ~5.5°C and 34.9 psu, respectively, with density lying between 1027.5 and 1027.6 kg m^{-3}; this corresponds to the $NADW_{on}$ states. The other cluster is markedly colder and fresher (0.5°C and ~32.6 psu) with a density range of 26.1–26.3 kg m^{-3}; this corresponds to the $NADW_{off}$ states. Therefore, $\rho_{NADW} > \rho_{AAIW}$ in the $NADW_{on}$ states and $\rho_{NADW} < \rho_{AAIW}$ in the $NADW_{off}$ states. The approximate T–S properties of an idealized mixture of AAIW and AABW are indicated by the dashed line in Fig. 7. This line varies between experiments, but for clarity only one line is shown here. NADW is only denser than the mixture of Antarctic water masses once AAIW dominates this mixture (approximately 75% AAIW, 25% AABW is required). Our experimental results suggest that a sufficiently deep DP is required to enable AAIW to dominate from the south. Otherwise, a shallow or closed DP sees dense AABW inhibiting the excitation of $NADW_{on}$ states, regardless of the AAIW densities.

c. Sensitivity to model experimental design

The critical depth of DP that enables NADW production to be sustained also depends in part on the particular thermal forcing used in the model. In our experiments, heat fluxes between the ocean and atmosphere resemble that of the present-day climate, resulting in a given set of THC equilibria as described above. However, if our model is forced using different surface heat fluxes, such as a colder North Atlantic, a different set of equilibria will emerge. To further assess this we have examined experiments wherein the southern bias of the thermal asymmetry between the AABW and NADW formation regions is reduced by applying a per-

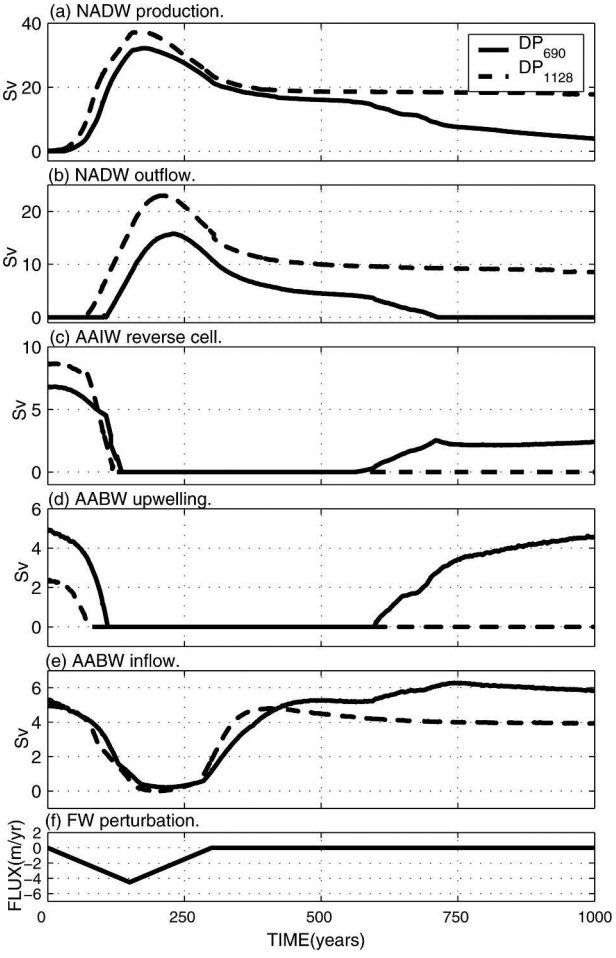

FIG. 6. Time-dependent behavior of (a) the magnitude of NADW production, (b) NADW outflow, (c) Atlantic AAIW reverse cell, (d) Atlantic AABW upwelling across 2000-m depth, (e) AABW inflow into the Atlantic, and (f) time history of FW perturbation (forcing 2) for DP_{1128} (dashed) and DP_{690} (solid). Definitions of the various MOT quantities are given in section 2c.

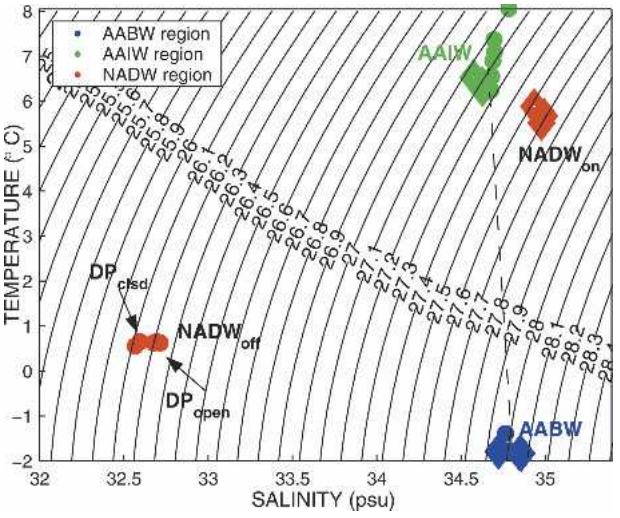

FIG. 7. Temperature–salinity properties at the sea surface in the sinking regions for all model equilibria of the present study. The colors correspond to the water mass formation regions shown in Fig. 1: AABW (blue), AAIW (green), and NADW (red). The $NADW_{off}$ states are indicated by dots and the $NADW_{on}$ states by diamonds. Contours of equal density (-1000 kg m^{-3}) in kg m^{-3} are overlaid. The dashed line indicates the approximate set of T–S values formed via an idealized mixture of AAIW and AABW. It is noted that the exact location of this line varies between experiments. See text for further details.

manent heat extraction of 200 W m^{-2} in the North Atlantic. This is undertaken in experiments DP_{clsd} and DP_{690}. New equilibria with only a small drop in global temperature are obtained as a new radiative balance with space is established. Application of forcing 2 to this heat-modified version of DP_{690} yields a transition to a stable $NADW_{on}$ state (note that this enhanced heat flux experiment also allows a stable $NADW_{off}$ state). The DP_{clsd} case, in contrast, does not sustain NADW production under these modified heat fluxes. Thus, caution should be taken when quantifying the critical depth for DP to enable excitation to $NADW_{on}$ states, because this critical depth depends, in part, on the global air–sea heat fluxes applied in the model. Under present-day thermal forcing, we have found that a critical DP depth of ~1000 m enables NADW to be sustained in a steady state.

Parameterization of subgrid-scale mixing is another factor that may influence the critical DP sill depth that is obtained in the model. We ran a DP_{clsd} experiment employing the subgrid-scale eddy parameterization of Gent and McWilliams (1990, hereafter GM) and found large rates of AABW formation (~44 Sv). As in our standard DP_{clsd} experiment, no stable NH overturning states could be excited in response to perturbations of the NA. In contrast, a DP_{open} case with GM mixing permits an $NADW_{on}$ state. This indicates that there must also be a critical DP sill depth that allows NADW formation to be sustained in experiments using GM. We have not explored a full DP depth series of experiments to identify this critical depth under GM. The important point is that such a depth exists, though its exact level will likely vary slightly according to model configuration.

4. Discussion

The North Atlantic freshwater perturbation experiments assessed in this study suggest that a DP_{clsd} geometry cannot sustain a stable NH overturning state under a present-day climate forcing. In DP_{clsd} the polarity and strength of the global MOT depends on the

interhemispheric density contrast between the high-latitude deep-water formation regions (as also noted by Rooth 1982; Bryan 1986). In Bryan's study the asymmetric overturning states are stable under symmetric surface forcing because a north–south salinity contrast is maintained by an interhemispheric MOT cell. In our model, surface thermal forcing is not symmetric—heat loss in the SH deep-water formation regions is significantly larger than that in the NH due to the local atmospheric forcing. The cold Antarctic conditions force a large SH sinking in DP_{clsd}.

Unless a dramatic cooling over the NA is artificially prescribed, none of the FW perturbations we employed could excite a transition to a state where ρ_{NADW} remains above ρ_{AABW} in a DP_{clsd} geometry. In the present-day climate $\rho_{AABW} > \rho_{NADW}$, and so NADW formation occurs by virtue of the existence of a deep DP that limits AABW production and sufficiently restricts the influence of this water mass to levels below 2000-m depth in the Atlantic. With the introduction of a DP gap, a third water mass, AAIW, enters the stage. Our results suggest that as DP deepens there is a gradual shift in importance from ρ_{AABW} to ρ_{AAIW} in the relation between SH surface density and ρ_{NADW}. Figure 7 shows that the $NADW_{on}$ states in the cases that permit multiple equilibria (DP_{1128}, DP_{1386}, and DP_{open}) are characterized by the relation $\rho_{NADW} > \rho_{AAIW}$. Saenko et al. (2003) stress the importance of this relationship in determining whether stable NADW sinking can occur. In our experiments the stability of the $NADW_{on}$ states appears to depend on the criteria that $\rho_{NADW} > \alpha \times \rho_{AAIW} + \beta \times \rho_{AABW}$, where α and β are mixing coefficients depending on the DP sill depth. Only in DP_{1128}, DP_{1386}, and DP_{open} is β sufficiently small for the relationship to hold.

The decreased influence of AABW that upwells above 2000-m depth in the Atlantic Ocean (Fig. 3) reveals the mechanism by which the shift in importance from ρ_{AABW} to ρ_{AAIW} occurs. When DP is shallow, there is significant upwelling of AABW to the surface in the Atlantic. This mass transport forms a closed cell that encompasses the surface layers and the AABW formation regions (Fig. 2b). This situation is similar to that of DP_{clsd}. In the shallow DP experiments (DP_{690} and DP_{896}), surface waters that are downwelled north of the DP gap recirculate to AABW formation regions (Fig. 2b), thereby sustaining the dominance of AABW on global MOT polarity. With deepening DP this mechanism of AABW dominance is impaired by an increasing obstruction for poleward geostrophic flow across the DP gap to the AABW formation regions. Water that is downwelled north of the DP exhibits an increasing preference for northward flow (as AAIW) instead of geostrophic flow to the south. This is because the downwelled water has more difficulty reaching the depths of the increasingly deep DP sill because of its buoyancy. The $NADW_{off}$ states displayed in Fig. 3 involve a gradual increasing preference (as DP deepens) for a northward branching of the water that is downwelled north of the circumpolar gap, thus, causing a gradual increase of AAIW inflow. This increase of AAIW inflow comes at the expense of AABW upwelling across 2000-m depth (Table 1). With more or less constant AABW inflow once DP is opened, AABW increasingly tends to recirculate below 2000-m depth as DP deepens (Fig. 3). The influence of ρ_{AABW} in the upper 2000 m is thus reduced, and it becomes possible for NADW to overlie the Atlantic variety of AABW. With an increasing amount of AAIW inflow, ρ_{AAIW} becomes a key factor in determining interhemispheric MOT patterns. At some stage a threshold occurs (in our experiments between DP sills at 896 and 1128 m) where the influence of the high ρ_{AABW} (due to cold conditions around Antarctica) becomes sufficiently reduced with respect to the lighter ρ_{AAIW} to allow a stable $NADW_{on}$ state. The observed reduction in NADW outflow for the stable $NADW_{on}$ states shown in Fig. 5 with decreased DP depth also results from a decreased southward branching of water that is downwelled north of the DP gap.

Global MOT polarity is determined by the sign of $[\alpha(D) \times \rho_{AABW} + \beta(D) \times \rho_{AAIW} - \rho_{NADW}]$ where D is the DP depth. However, ρ_{AAIW} also affects the penetration depth of AAIW. The fraction of north/south branching in the bifurcation of water that is downwelled north of DP is determined by the DP depth and by the buoyancy of the downwelled water. Therefore, a change in ρ_{AAIW} while D remains constant can also affect the bifurcation. This means that α and β are functions of ρ_{AAIW} as well as D. We find, however, that ρ_{AAIW} remains relatively constant across experiments with changes in D (see Fig. 7). This means that the bifurcation rates depend almost exclusively on the DP depth in our experiments.

We assessed the role of surface heat flux forcing in determining the critical threshold DP depth for NADW formation to be sustained. Under a present-day heat flux forcing scenario, this critical DP depth appears to be around 1000 m. However, different heat flux scenarios, such as a cooler NA, see different threshold DP depths. For example, a sufficiently high ocean heat loss in the NA is found to permit a stable $NADW_{on}$ state in the DP_{690} geometry. From a paleoclimate perspective, this suggests that while the DP depth controls the existence of multiple ocean equilibria, there is no single threshold depth that characterizes all climate states.

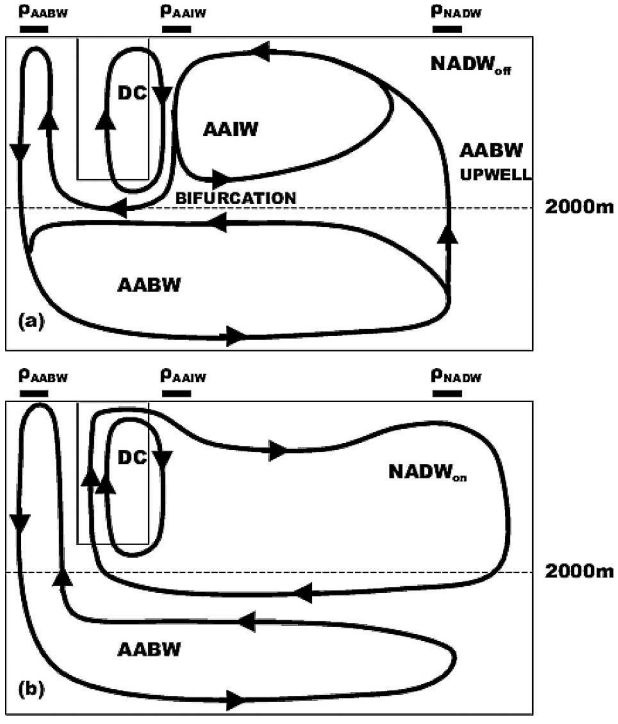

FIG. 8. Schematic representation of the Atlantic meridional overturning with DP open to its present-day depth for (a) the $NADW_{off}$ and (b) the $NADW_{on}$ states. The water mass formation regions are indicated at the surface; DC indicates the Deacon Cell.

Figure 8 shows a schematic diagram of the $NADW_{off}$ and $NADW_{on}$ states with DP at its present-day depth. Note the bifurcation in the downwelling route north of the DP gap in $NADW_{off}$. The fraction of mass in each part of the bifurcation regulates the relative importance of ρ_{AABW} and ρ_{AAIW}; greater northward branching (as occurs once DP is deep) shifts the emphasis to ρ_{AAIW}. Increasing the DP depth strengthens the northward branch at the expense of the southward branch in the bifurcation. The $NADW_{on}$ state is completely different, with no reverse cell of AAIW and NADW forming a closed cell that encompasses the Deacon Cell. In addition, no AABW is upwelled across 2000-m depth in $NADW_{on}$, even though the AABW inflow appears relatively unchanged between the $NADW_{off}$ and $NADW_{on}$ states.

5. Conclusions

We have shown that NADW formation and stability depend critically on the depth of the DP sill via the interplay between northern and southern water masses. As DP deepens a greater component of AAIW flows to the north of its formation region, shifting the AABW–NADW competition in DP_{clsd} to one that combines the more buoyant AAIW mass. This eventually enables NADW to form stably once a critical DP depth is reached.

Models resolving a net mass transport across the ACC induced by mesoscale eddies allow an increased shallow southward conduit for water originating north of the DP gap. Gnanadesikan (1999) refers to this as the "eddy return flow" in his elegant model and finds a negative effect on NADW formation through a shoaling of the pycnocline. By analogy, our results show that an increased southward conduit occurs when DP is shallow, which in turn increases AABW upwelling across 2000 m and strengthens the importance of that water mass in controlling the global MOT.

Further examination of the effect of the DP gap on global climate could include systematic vatiations in the hydrological cycle as well as the thermal conditions in the Northern and Southern Hemispheres, employing varying geometries with different DP depths. In this study, we have shown that the depth of the DP sill is of first order importance in controlling the stability of the ocean's global thermohaline circulation.

Acknowledgments. The authors are grateful to the University of Victoria, Andrew Weaver, Oleg Saenko, and Michael Eby for supplying us with the Earth System Climate Model, and for invaluable technical and scientific advice regarding its use. Comments by Andreas Schmittner and an anonymous reviewer are also gratefully acknowledged. This research was supported by the Australian Research Council and Australia's Antarctic Science Program.

REFERENCES

Broecker, W., S. Sutherland, and T. Peng, 1999: A possible 20th-century slowdown of Southern Ocean deep water formation. *Science,* **286,** 1132–1135.

Bryan, K., 1986: High-latitude salinity effects and interhemispheric thermohaline circulation. *Nature,* **323,** 301–304.

Cox, M. D., 1989: An idealized model of the World Ocean. Part I: The global-scale water masses. *J. Phys. Oceanogr.,* **19,** 1730–1752.

Döös, K., and D. J. Webb, 1994: The Deacon cell and the other meridional cells in the Southern Ocean. *J. Phys. Oceanogr.,* **24,** 429–442.

Duffy, P. B., and K. Caldeira, 1997: Sensitivity of simulated salinity in a three-dimensional ocean model to upper-ocean transport of salt from sea-ice formation. *Geophys. Res. Lett.,* **24,** 1323–1326.

England, M. H., J. S. Godfrey, A. C. Hirst, and M. Tomczak, 1993: The mechanism for Antarctic Intermediate Water renewal in a World Ocean model. *J. Phys. Oceanogr.,* **23,** 1553–1560.

Gent, P. R., and J. C. McWilliams, 1990: Isopycnal mixing in ocean general circulation models. *J. Phys. Oceanogr.,* **20,** 150–155.

Gnanadesikan, A., 1999: A simple predictive model for the structure of the oceanic pycnocline. *Science,* **283,** 2077–2079.

——, and R. W. Hallberg, 2000: On the relationship of the Circumpolar Current to Southern Hemisphere winds in coarse-resolution ocean models. *J. Phys. Oceanogr.,* **30,** 2013–2034.

Kennett, J. P., 1977: Cenozoic evolution of Antarctic glaciation, the Circum Antarctic Ocean, and their impact on global paleoceanography. *J. Geophys. Res.,* **82,** 3843–3860.

Klinger, B. A., S. Drijfhout, J. Marotzke, and J. R. Scott, 2004: Remote wind-driven overturning in the absence of the Drake Passage effect. *J. Phys. Oceanogr.,* **34,** 1036–1049.

McCartney, M. S., 1977: Subantarctic mode water. *A Voyage of Discovery*, M. V. Angel, Ed., Pergamon, 103–119.

Rahmstorf, S., and M. H. England, 1997: On the influence of Southern Hemisphere winds on North Atlantic deep water flow. *J. Phys. Oceanogr.,* **27,** 2040–2054.

Rooth, C., 1982: Hydrology and ocean circulation. *Progress in Oceanography,* Vol. 11, Pergamon, 131–149.

Saenko, O. A., A. J. Weaver, and J. M. Gregory, 2003: On the link between the two modes of the ocean thermohaline circulation and the formation of global-scale water masses. *J. Climate,* **16,** 2797–2801.

Sijp, W. P., and M. H. England, 2004: Effect of the Drake Passage throughflow on global climate. *J. Phys. Oceanogr.,* **34,** 1254–1266.

Toggweiler, J. R., and B. Samuels, 1995: Effect of Drake Passage on the global thermohaline circulation. *Deep-Sea Res.,* **42A,** 477–500.

——, and H. Bjornsson, 2000: Drake Passage and paleoclimate. *J. Quat. Sci.,* **15,** 319–328.

Tsujino, H., and N. Suginohara, 1999: Thermohaline circulation enhanced by wind forcing. *J. Phys. Oceanogr.,* **29,** 1506–1516.

Weaver, A. J., and Coauthors, 2001: The UVic Earth System Climate Model: Model description, climatology and applications to past, present and future climates. *Atmos.–Ocean,* **39,** 361–428.